Finite element modelling of cold drawing for high-precision tubes

Florian Boutenel, Myriam Delhomme, Vincent Velay, Romain Boman

▶ **To cite this version:**

Florian Boutenel, Myriam Delhomme, Vincent Velay, Romain Boman. Finite element modelling of cold drawing for high-precision tubes. Comptes Rendus Mécanique, 2018, 346 (8), pp.665-677. 10.1016/j.crme.2018.06.005 . hal-01822637

HAL Id: hal-01822637

https://imt-mines-albi.hal.science/hal-01822637

Submitted on 25 Jun 2018

HAL is a multi-disciplinary open access archive for the deposit and dissemination of scientific research documents, whether they are published or not. The documents may come from teaching and research institutions in France or abroad, or from public or private research centers.

L'archive ouverte pluridisciplinaire **HAL**, est destinée au dépôt et à la diffusion de documents scientifiques de niveau recherche, publiés ou non, émanant des établissements d'enseignement et de recherche français ou étrangers, des laboratoires publics ou privés.

Distributed under a Creative Commons Attribution - NonCommercial - NoDerivatives 4.0 International License

C. R. Mecanique ••• (••••) •••–•••

Contents lists available at ScienceDirect

Comptes Rendus Mecanique

www.sciencedirect.com

Computational modeling of material forming processes / Simulation numérique des procédés de mise en forme

Finite element modelling of cold drawing for high-precision tubes

Florian Boutenel [a,*], Myriam Delhomme [b], Vincent Velay [a], Romain Boman [c]

[a] ICA (Institut Clément-Ader), Université de Toulouse, CNRS, IMT Mines Albi, INSA, UPS, ISAE–SUPAERO, Campus Jarlard, 81013 Albi CT cedex 09, France
[b] Minitubes ZAC Technisud, 21, rue Jean-Vaujany, BP 2529, 38035 Grenoble cedex 02, France
[c] Department of Aerospace and Mechanical Engineering, University of Liège, 9, allée de la Découverte, B-4000 Liège, Belgium

ARTICLE INFO

Article history:
Received 29 August 2017
Accepted 9 January 2018
Available online xxxx

Keywords:
Precision metal forming
Cold tube drawing
Tube sinking
Mandrel drawing
Finite element method
Large deformation

ABSTRACT

Cold tube drawing is a metal forming process that allows manufacturers to produce high-precision tubes. The dimensions of the tube are reduced by pulling it through a conical converging die with or without inner tool. In this study, finite element modelling has been used to give a better understanding of the process.

This paper presents a model that predicts the final dimensions of the tube with very high accuracy. It is validated thanks to experimental tests. Moreover, five studies are performed with this model, such as investigating the influence of the die angle on the drawing force or the influence of relative thickness on tube deformation.

© 2018 Académie des sciences. Published by Elsevier Masson SAS. This is an open access article under the CC BY-NC-ND license (http://creativecommons.org/licenses/by-nc-nd/4.0/).

1. Introduction

Medical devices, like stents, cardiac valves, and implants, are manufactured with thin-walled tubes of small diameters [1]. As applications in the biomedical field, these tubes require a very high precision in dimensions and surface finish. Also, these properties are strongly linked to the quality of the metal forming process.

Cold tube drawing enables manufacturers to produce tubes with controlled dimensions, good surface finish, and high mechanical properties [2]. This metal forming process gives a better tube quality compared to hot forming. Tube drawing consists in reducing the tube dimensions by pulling it through a conical converging die with or without inner tool. Different drawing methods exist [3]. In this paper, two techniques are studied: tube sinking and mandrel drawing (Fig. 1).

For both of them, the die calibrates the tube's outer diameter. Tube sinking is the only method that does not use an inner tool. The inner diameter is reduced because of the free deformation inside the tube. In consequence, the inner surface finish is degraded. In mandrel drawing, the inner tool, named mandrel, moves with the tube and calibrates its inner diameter. The main drawback of this technique is related to the end of the drawing operation where the tube is clamped around the mandrel. Thus, a reeling operation is required to remove the tool.

The metal forming industry wants to perpetually improve productivity and product quality. In order to reach this purpose, a better understanding of the processes is necessary. On the one hand, a large series of experimental tests can be done.

* Corresponding author.
E-mail addresses: florian.boutenel@mines-albi.fr (F. Boutenel), m.delhomme@minitubes.com (M. Delhomme), vincent.velay@mines-albi.fr (V. Velay), r.boman@ulg.ac.be (R. Boman).
URLs: http://www.institut-clement-ader.org/ (F. Boutenel and V. Velay), http://www.minitubes.com/ (M. Delhomme), http://www.ltas-mnl.ulg.ac.be/ (R. Boman).

https://doi.org/10.1016/j.crme.2018.06.005
1631-0721/© 2018 Académie des sciences. Published by Elsevier Masson SAS. This is an open access article under the CC BY-NC-ND license (http://creativecommons.org/licenses/by-nc-nd/4.0/).

Please cite this article in press as: F. Boutenel et al., Finite element modelling of cold drawing for high-precision tubes, C. R. Mecanique (2018), https://doi.org/10.1016/j.crme.2018.06.005

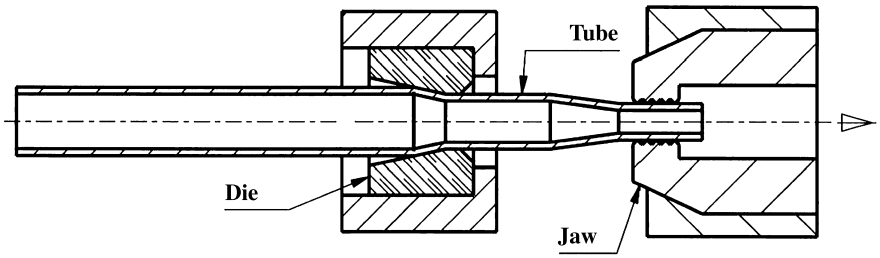

(a) Tube sinking.

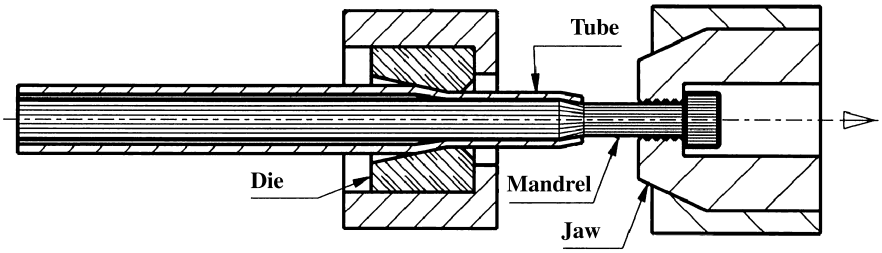

(b) Mandrel drawing.

Fig. 1. Sketch of the two drawing methods studied in this paper (adapted from [4]).

However, this type of approach may be time and money consuming. On the other hand, lots of tests can be performed virtually thanks to finite element (FE) modelling. It also gives access to physical values, such as stresses and strains, which are not measurable during the process. Thus, FE modelling seems to be a helpful tool.

Analytical solutions have been developed by several authors to study the effects of process parameters. Um et al. [5] obtained an upper bound solution to fixed plug drawing that can be simplified in the case of tube sinking. This method has been adapted to mandrel drawing by Alexandrova [6] in the case of mandrel drawing. Later, the Hill's general method of analysis for metalworking processes and a fracture criterion have been added to this analytical model to study the workability of mandrel drawing [7]. Zhao et al. [8] have proposed an analytical solution to tube sinking using an integration method of strain rate vector inner product.

Numerical studies of tube drawing using FE can also be found in the literature. A finite element analysis has been conducted by Sawamiphakdi et al. [9] to determine the initial tube sizes that give the appropriate mechanical properties after drawing. Linardon et al. [10] combined a conical mandrel tube drawing test with a FE modelling to select a failure criterion. The potential making of high-quality thin tubes with shape-memory alloys thanks to mandrel drawing has been studied by Yoshida et al. [3]. Karnezis et al. [11] used a FE model to investigate the possibility of reducing the number of drawing passes. Palengat et al. [12] underlined the importance of the properties of the interface (tube with tools) on the drawing limits. Several studies dealing with tools design have been achieved in order to improve the process. Sheu et al. [13], Lee et al. [14] and Béland et al. [15] focused on the die geometry, while Kim et al. [16] had an interest for the mandrel one.

In this paper, a FE model is designed to precisely predict the final dimensions of the tube. This axisymmetric steady-state model takes into account different issues, including tool geometry, tube elastoviscoplastic behaviour, tool elastic behaviour, contacts and friction. Moreover, the numerical convergence is built to reach a 1-micron accuracy. In consequence, this model can be used to analyse the tube drawing process, and thus, permits a better understanding.

This modelling was performed on Metafor [17–19], an in-house nonlinear finite element code of the Department of Aerospace and Mechanical Engineering of the University of Liège, Belgium.

This paper is organised as follows. A detailed model formulation is given in Section 2. Then, Section 3 compares the numerical results with drawing experiments in order to validate the model. Furthermore, a numerical analysis of the process is presented in Section 4. Finally, Section 5 reports on the conclusions of this work.

2. Formulation of the finite element model

This section describes precisely the FE modelling. Tube sinking and mandrel drawing are treated together because of their many similarities. For mandrel drawing, the reeling operation is not modelled. It implies that, at the end of the simulation, the tube remains clamped around the mandrel.

Please cite this article in press as: F. Boutenel et al., Finite element modelling of cold drawing for high-precision tubes, C. R. Mecanique (2018), https://doi.org/10.1016/j.crme.2018.06.005

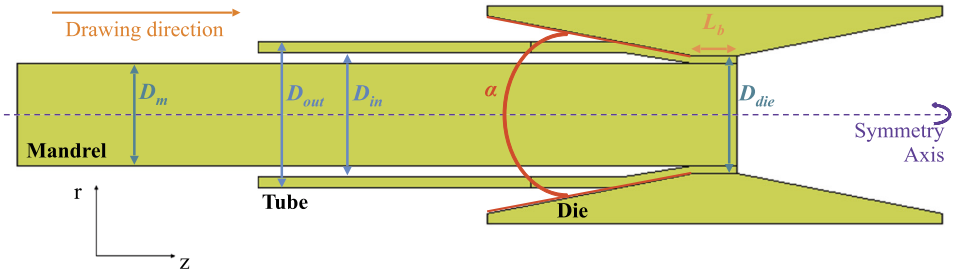

Fig. 2. Geometry of the model (mandrel drawing case).

Table 1
Chemical composition of the 316LVM stainless steel (ASTM-F138 [20]).

Element	Fe	Cr	Ni	Mo	Mn	Si	Cu	N	C	P	S
Mass %	Balance	17–19	13–15	2.25–3	<2	<0.75	<0.5	<0.1	<0.03	<0.025	<0.01

2.1. Geometry

By assumption, the tube and the tools are geometrically perfect. These elements are also supposed to be coaxial. Moreover, the geometry and the loading conditions have an axial symmetry. Thus, the process is axisymmetric and can be solved in 2D.

First, the tube is described by its outer and inner diameters (respectively D_{out} and D_{in}). Then, the die geometry includes various dimensions: the diameter D_{die}, the bearing length L_{b}, the entry die angle α. In the case of mandrel drawing, the inner tool is represented by its diameter D_{m}.

The geometry of the model is given in Fig. 2. In practice, the beginning of the tube is inserted in the die before starting the drawing operation. The results of this area are not relevant. Besides, even if the die seems to be symmetric, the tool is not reversible. In fact, the die holder ensures that the die is used in the correct way.

2.2. Materials

In this model, the tube and the tools are both represented by deformable solids.

The tube is made of 316LVM stainless steel. This material is commonly used for biomedical applications because of its excellent resistance to various types of corrosion. Its chemical composition is given in Table 1.

Palengat et al. [12] observed an isotropic behaviour of this material. Then, Fréchard et al. [21] showed that:

- at ambient temperature (temperature of the process), nitrogen-alloyed austenitic stainless steels are strain-rate sensitive;
- the viscoplastic model of Johnson–Cook is the most appropriate to describe the behaviour of these materials at different strain rates.

The constitutive equation of this model [22] is:

$$\sigma_{\text{eq}} = \left(A + B\varepsilon_{\text{eq}}^{n}\right)\left(1 + C\ln\frac{\dot{\varepsilon}_{\text{eq}}}{\dot{\varepsilon}_{\text{eq}}^{0}}\right)\left(1 - \left(\frac{T - T_{\text{ref}}}{T_{\text{m}} - T_{\text{ref}}}\right)^{m}\right) \tag{1}$$

where σ_{eq} represents the flow stress, ε_{eq} the equivalent plastic strain, A the yield stress, B the pre-exponential factor, $\dot{\varepsilon}_{\text{eq}}$ the plastic strain rate, $\dot{\varepsilon}_{\text{eq}}^{0}$ the reference plastic strain rate, C the strain rate sensitivity coefficient, n the work-hardening coefficient, T the temperature of the material, T_{m} the melting temperature of the material, T_{ref} the reference temperature, and m the thermal softening exponent. In other words, the first factor is related to work hardening, the second one to strain rate dependence, and the last one to thermal softening.

However, the thermal softening term can be neglected if the strain rate of the process does not allow the material to be affected by the temperature rise [23]. On one side, the strain rate in cold drawing process can reach 40 s^{-1}. On the other one, the experimental measures showed that the tube temperature does not exceed 130 °C [12], i.e. less than one tenth of the material's melting point (1400 °C). Thus, the thermal softening term can be safely neglected in (1). Finally, the von Mises yield criterion is used to model plasticity.

The mechanical properties and the Johnson–Cook parameters of 316LVM are respectively listed in Tables 2 and 3. A representation of the Johnson–Cook law is also given in Fig. 3.

The die is made of tungsten carbide, while the mandrel is made of steel. Both materials are considered as isotropic. During the process, no irreversible deformation is observed in the tools, so the behaviour is assumed to be perfectly elastic during drawing. The mechanical properties of the materials of which the tools are made of are listed in Table 4.

Please cite this article in press as: F. Boutenel et al., Finite element modelling of cold drawing for high-precision tubes, C. R. Mecanique (2018), https://doi.org/10.1016/j.crme.2018.06.005

Table 2
Mechanical properties of the material of which the tube is composed.

Density	Young's modulus	Poisson's ratio
7 900 kg·m^{-3}	192 GPa	0.29

Table 3
Johnson–Cook parameters of 316LVM stainless steel [24].

A	B	C	n	$\dot{\varepsilon}^0_{eq}$
287 MPa	1265 MPa	0.021	0.664	0.03 s^{-1}

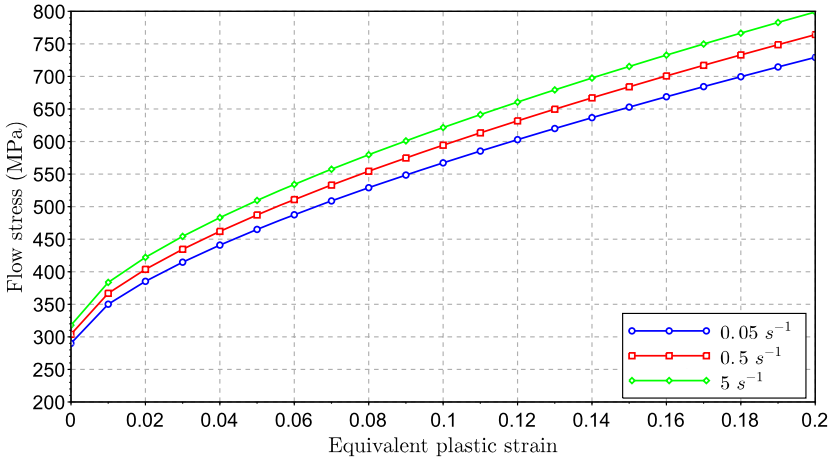

Fig. 3. Representation of the Johnson–Cook law for 316LVM stainless steel for three plastic strain rates (with parameters of Table 3).

Table 4
Mechanical properties of the materials of which the tools are composed.

	Tungstene carbide	Steel
Density (kg·m^{-3})	15 000	7 900
Young's modulus (GPa)	650	210
Poisson's ratio	0.3	0.3

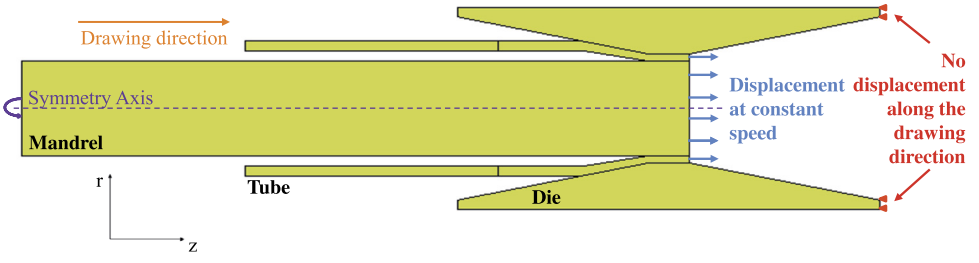

Fig. 4. Boundary conditions of the model (mandrel drawing case).

2.3. Boundary conditions

Two boundary conditions are prescribed in this model (Fig. 4).

The right-hand extremity of the die is fixed along the drawing direction in order to model the contact with the die holder. Then, a displacement condition is applied to the tube and the mandrel, if it exists. This displacement is prescribed at constant speed. It corresponds to the steady speed of the drawing trolley.

2.4. Contact

Two contact pairs should be taken into account: tube/die and tube/mandrel.

Please cite this article in press as: F. Boutenel et al., Finite element modelling of cold drawing for high-precision tubes, C. R. Mecanique (2018), https://doi.org/10.1016/j.crme.2018.06.005

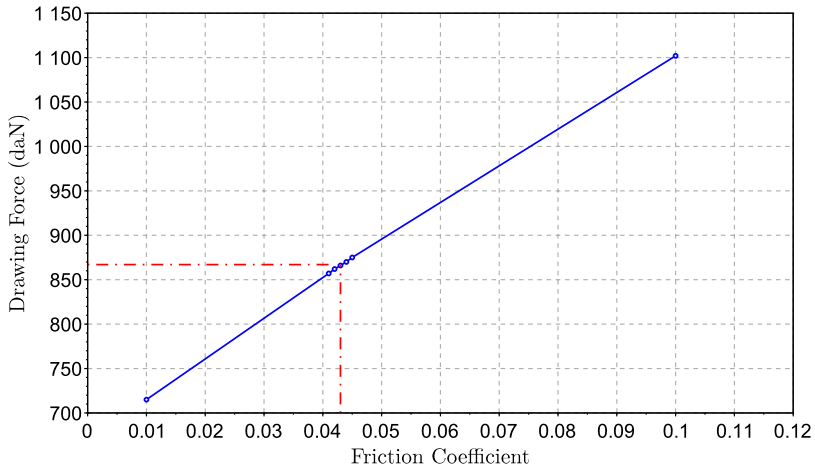

Fig. 5. Drawing force evolution as a function of the friction coefficient $\mu_{\text{tube/die}}$ (tube sinking case).

Table 5
Friction coefficients identified by inverse analysis.

$\mu_{\text{tube/die}}$	$\mu_{\text{tube/mandrel}}$
0.043	0.139

In the industrial process, lubrication is used to reduce friction between each part. By assumption, it is homogeneous and constant.

Friction depends on several parameters: materials in contact, relative velocity, surface roughness, thickness of the oil film, normal pressure, etc. In this study, the contacts are described by a Coulomb friction model. Thus, two friction coefficients are defined: $\mu_{\text{tube/die}}$ and $\mu_{\text{tube/mandrel}}$. However, these coefficients are difficult to measure in practice. In consequence, an inverse analysis is used to identify them.

For each case, representative tests were performed experimentally and then, simulated with various friction coefficients. A nearly linear dependence was observed between the drawing force and the friction coefficient (Fig. 5).

The coefficient, which permits us to match the simulated force with the measured one, was kept for the whole study. $\mu_{\text{tube/die}}$ was firstly identified thanks to a tube sinking test. This coefficient is assumed to be the same in both drawing methods. Then, a mandrel drawing test allowed us to determine $\mu_{\text{tube/mandrel}}$. The values of the friction coefficients are listed in Table 5.

These values fit in the range of those of the literature concerning cold tube drawing. In fact, usual coefficients are included between 0.03 [3] and 0.2 [25].

2.5. Mesh

The tube and the tools are meshed with 4-node-quadrangular elements using selective reduced integration (SRI), meaning that the pressure increment over an element is constant and computed at the centre of the element. While the deviatoric part of the stress tensor is evaluated at 4 Gauss points. Fig. 6 shows a view of the initial mesh. In practice, only the upper half of the model (above the symmetric axis) is meshed and solved by the finite element method. Moreover, it could be mentioned that there is no contact between the tube and the tool on the right-hand part (corresponding to the tool area after the output plane in Fig. 6). However, in order to simplify the mesh procedure and not to add another numerical parameter into the study (Section 2.6.2), the right-hand part of the tool is meshed in the same way as the left-hand part is.

2.6. Analysis of numerical factors

This finite element model includes various numerical methods using different parameters. These methods are related to the contact algorithm, the mesh, the integration time, and the required duration of the simulation to reach the steady state. Also, the parameters are chosen to assure a reliability of the model. In fact, all the following numbers result from a numerical study and ensure the best compromise between CPU time and the desired 1-micron accuracy (see Section 2.6.5).

2.6.1. Contact

Both contact pairs (tube/die and tube/mandrel) are numerically managed by the same methods using identical sets of parameters.

Please cite this article in press as: F. Boutenel et al., Finite element modelling of cold drawing for high-precision tubes, C. R. Mecanique (2018), https://doi.org/10.1016/j.crme.2018.06.005

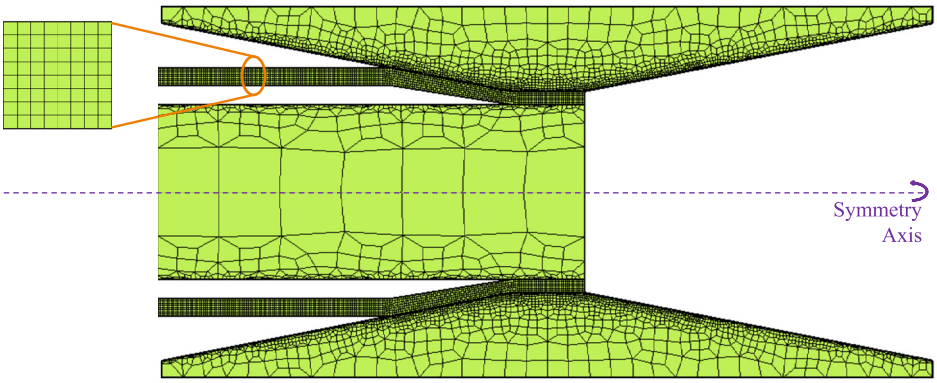

Fig. 6. Initial mesh of the model (mandrel drawing case).

A penalty contact algorithm [18] is used. The penalty coefficient along the normal direction is equal to 10^7 MPa·mm^{-1}. Along the tangential direction, the coefficient is defined as the normal one multiplied by the friction coefficient. This means that the geometrical error is identical along both directions when the surfaces slide over each other.

Finally, the contact is modelled as a node-to-surface contact using a single-pass method [19]. This implies that master and slave surfaces have to be assigned. On one side, the master surface corresponds to the more rigid one. Thus, in each case, the surface of the tool is considered as the master surface. On the other one, the slave surface is assigned to the tube. Moreover, the depth, at which the detection occurs is equal to half a tube thickness.

2.6.2. Mesh

The tube is meshed with 8 square elements in its thickness. This number is coherent with other studies. For instance, Palengat et al. [12] have used at least 8 elements in the thickness to study the forming limit.

In order to consume less CPU time, the tools are meshed with larger elements. In fact, the global size of the elements has been chosen to be ten times bigger in the die core than in the tube. This factor is equal to thirty for the mandrel. However, the mesh of the tools is refined near the contact zones in order to avoid contact between segments with very different lengths. As previously, a size factor is defined: 0.5 for the die and 2 for the mandrel.

2.6.3. Time integration

A Chung–Hulbert scheme [26] is used for time integration. This implicit dynamic integration scheme belongs to the generalised α-scheme family.

Then, the time increment is limited by a user-defined maximum value in order to ensure that the tube deformation is progressive and remains small during each increment. In this way, this value is defined so that a node covers the length of a tube element in 25 steps. Although the resulting size of the time increment is rather small, it is significantly larger than the one expected with an explicit approach. Moreover, using the proposed implicit method, compared to an explicit one, prevents us from managing additional numerical parameters such as mass and load scaling factors and hourglass control.

Finally, the equilibrium tolerance within each increment is set to 10^{-4} to assure a convergence without too much CPU time consumption.

2.6.4. Steady state

The duration of the simulated process is set so that the whole tube is drawn and leave the die so that the springback is modelled.

Also, the modelled tube length should be sufficient to reach the steady-state conditions far from tube ends during drawing. In this way, a minimum length of 20 mm should be considered.

2.6.5. Analysis method

All the previous parameters were set in order to guarantee the reliability of the model. The approach that has been used is explained in this paragraph.

A parameter is chosen: for instance, the penalty coefficient along the normal direction. This coefficient expresses, numerically, the stiffness of the contact. This means that the greater it is, better the contact is represented.

Next, the value of this parameter is changed, while the others are fixed. Table 6 gives an example of results.

According to the previous definition of this coefficient, the largest value (10^8 MPa·mm^{-1}) is taken as the reference. An error of 39.3 µm is observed on the outer diameter if the coefficient is set to 10^4 MPa·mm^{-1}. This error is bigger than the micron accuracy which is expected. Thus, a coefficient of 10^6 or 10^7 MPa·mm^{-1} allows us to verify this accuracy while consuming less time than the reference. Finally, the value of 10^7 MPa·mm^{-1} was chosen for the rest of the study.

Please cite this article in press as: F. Boutenel et al., Finite element modelling of cold drawing for high-precision tubes, C. R. Mecanique (2018), https://doi.org/10.1016/j.crme.2018.06.005

Table 6
Analysis method to elect the best penalty coefficient used by the contact algorithm along the normal direction (tube sinking case).

Penalty coefficient ($MPa{\cdot}mm^{-1}$)	Drawing force (daN)	Outer diameter (mm)	Thickness (mm)	CPU time
10^4	854	7.0565	0.9839	54 min 30 s
10^5	864	7.0207	0.9825	54 min 33 s
10^6	866	7.0176	0.9822	55 min 21 s
10^7	866	7.0172	0.9821	58 min 53 s
10^8	867	7.0172	0.9821	1 h 43 min

Table 7
Tools dimensions.

Test	Die			Mandrel
	D_{die} (mm)	L_b (mm)	α (deg)	D_m (mm)
1	7.012	2.010	14.859	–
2	6.64	2.4	22.0	5.80

3. Model validation with drawing experiments

Various drawing tests were performed on industrial benches in order to validate the model. Two of them are presented in this section.

3.1. Experiments

Test 1, performed for this paper, deals with tube sinking. A tube (D_{out} = 9.88 mm and D_{in} = 8.07 mm) is pulled through a die of 7.01 mm of diameter. This corresponds to an area reduction of 28%. Test 2, extracted from another work [4], concerns mandrel drawing. The section area of a tube (8.16 mm × 7.05 mm) is reduced by 38% using a die (D_{die} = 6.64 mm) and a mandrel (D_m = 5.80 mm).

3.1.1. Measurements

The tube dimensions were precisely measured before and after the drawing operation. The outer diameter was given by a laser measure (three points on two sections of the tube). An Heidenhain touch probe was used to measure the thickness on eight points of one tube section. The inner diameter was then deduced.

The dimensions of the die were measured thanks to a Mitutoyo coordinate measuring machine.

As the outer diameter of the tube, the mandrel diameter was measured thanks to a laser. In the case of mandrel drawing, given the fact that the reeling operation is not simulated, the tube is clamped around the mandrel at the end of the process. As a consequence, the measure of the tube outer diameter was done with the mandrel inside. Also, the thickness was deduced by assuming that the tube's inner diameter is equal to the mandrel's diameter. Tools measurements are listed in Table 7.

The tests were performed at ambient temperature (22 °C) and at constant speed (9.37 $m{\cdot}min^{-1}$ for Test 1 and 11.4 $m{\cdot}min^{-1}$ for Test 2).

3.1.2. Results

During the tests, the drawing force was measured by a load cell located between the die and the die holder. Fig. 7 gives the evolution of the force during drawing.

Three stages can be discerned. At the beginning of the drawing (at $t = 0$ s), the force increases quickly. Then, a mechanical steady state is defined by a constant force. At $t = 12.3$ s, the tube gets out of the die (end of drawing), and the force becomes zero. Such evolution can be observed for all drawings.

The drawing tests results are summarised in Table 8.

3.2. Comparison with the FE model

Both tests were simulated with the finite element model described in Section 2. This allowed us to calculate the drawing force, the outer diameter, and the final thickness of the tubes.

In order to be consistent with the experimental measurements, the numerical drawing force is calculated as the reaction force on the fixed side of the die (see Fig. 4). The diameter and the thickness are calculated on a tube section that is not submissive to side effects.

Results of FE simulations are included in Table 9.

Please cite this article in press as: F. Boutenel et al., Finite element modelling of cold drawing for high-precision tubes, C. R. Mecanique (2018), https://doi.org/10.1016/j.crme.2018.06.005

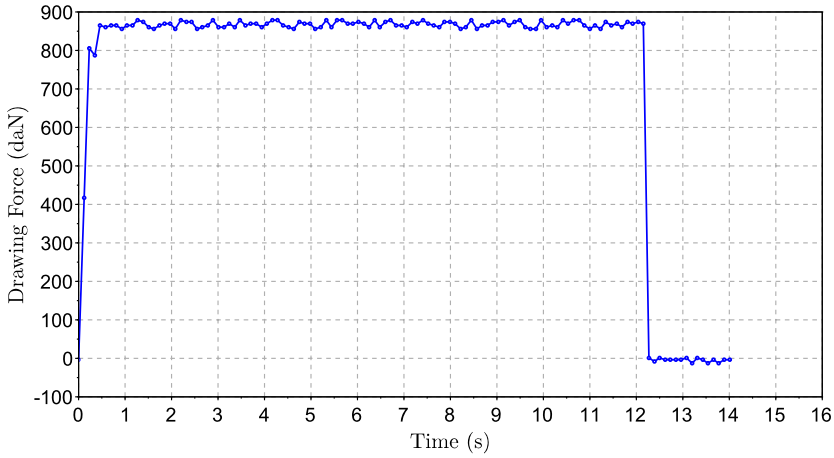

Fig. 7. Evolution of the experimental drawing force (Test 1).

Table 8
Results of the experimental drawing tests.

Test	Initial tubes (mm)			Final tubes (mm)			Drawing force (daN)
	Outer ∅	Thickness	Inner ∅	Outer ∅	Thickness	Inner ∅	
1	9.875 ±0.002	0.901 ±0.002	8.073	7.019 ±0.0005	0.959 ±0.003	5.101	867 ±11
2	8.16 ±0.002	0.555 ±0.002	7.05	6.6726 ±0.001	5.80	0.4363	739 ±23

Table 9
Comparison between experimental (EXP) and FE results.

Test		Drawing force (daN)	Outer diameter (mm)	Thickness (mm)
1	EXP	867	7.019	0.959
	FE	866	7.0172	0.9821
	Difference	1	−0.0018	+0.0231
		0.1%	0.03%	2.41%
2	EXP	739	6.6726	0.4363
	FE	739	6.6689	0.4423
	Difference	0	−0.0037	+0.006
		<0.1%	0.06%	1.38%

Table 10
CPU statistics.

Test	Real drawing time (s)	CPU time	Number of steps
1	0.285	53 min 48 s	9994
2	0.208	4 h 26 min	18511

As expected, the calculated drawing force is quite equal to the measured one. In fact, the friction coefficients, identified in Table 5, allow us to obtain this result.

In both tests, the outer diameter and the thickness are well predicted.

These simulations have used an Intel Core i7 3.20 GHz processor. The CPU statistics are listed in Table 10.

In conclusion, this comparison with drawing experiments shows that the presented model is able to predict the final dimensions of the tube with a good accuracy.

4. Numerical analysis of the process

The validated model can be used to give a better understanding of the cold tube drawing process. In this purpose, five studies are presented in this section.

Please cite this article in press as: F. Boutenel et al., Finite element modelling of cold drawing for high-precision tubes, C. R. Mecanique (2018), https://doi.org/10.1016/j.crme.2018.06.005

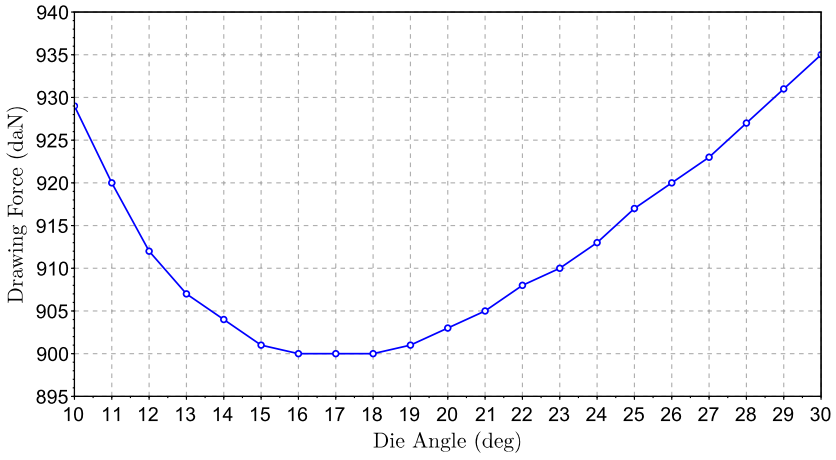

Fig. 8. Drawing force as a function of the die angle (tube sinking case).

4.1. Influence of the die angle on the drawing force

The required pulling force to draw a tube is a critical value in the design of the industrial process, because it calibrates the capacity of the bench. Thus, it is interesting to know the influence of process parameters on the force.

In particular, the entry die angle is strongly linked to it. In this way, a tube sinking simulation was repeated with various angle values (from 10° to 30° by step of 1°). The other parameters are those of Test 1 (see Table 7). The variations of the drawing force are shown in Fig. 8. Also, the equivalent plastic strain is given in Fig. 9 for three values of the die angle.

Béland et al. [15] revealed that an optimum value of the die angle minimises the drawing force. This result can be observed here for $\alpha = 17°$.

When the die angle deviates from the optimum value, the force increases. However, a dissymmetry is observed because the increase, on either side of the optimum value, does not have the same origin. When the die's angle is below the optimum value, the friction predominates over the deformation. If the angle decreases, the friction between the tube and the die increases and so the force increases. When the die's angle is above the optimum value, deformation predominates over friction. If the angle increases, the tube must deform more in order to keep a constant material flow. As a consequence, a greater force is needed.

Finally, Fig. 9 shows that the equivalent plastic strain of the tube increases with the die angle. Furthermore, the model predicts that, in the presented cases of tube sinking, no contact occurs between the tube and the die along the bearing length. Due to a scale effect, this observation is more visible in Fig. 9(c).

4.2. Influence of the initial relative thickness on the geometry of the tube

Various tube thicknesses could be drawn through a given die. As a consequence, a dimensionless quantity is used to compare the different kinds of drawings. The relative thickness of the tube is defined as the ratio between the thickness and the outer radius.

During drawing, the tube deformation is directly influenced by its initial relative thickness. Fig. 10 shows the variation rate of thickness as a function of the relative thickness, for tube sinking. This graph is obtained by repeating the simulation of Test 1 with various values of the initial inner diameter of the tube in order to reach a wide range of relative thicknesses.

When the initial relative thickness increases, the variation rate of the thickness decreases. Also, in the presented case, the thickness is not modified by the drawing operation if the dimensionless quantity is equal to 40%. So, two behaviours can be distinguished. If the relative thickness is below 40%, the variation rate is positive. In other words, the tube gets thicker after drawing. If the relative thickness is above 40%, the variation rate is negative, and so, due to drawing, tube thickness decreases. This behaviour is commonly observed in practice in the industry.

4.3. Influence of the initial relative thickness on the elongation

As the drawing process implies a diameter reduction, the tube is stretched. In this study, the influence of the initial relative thickness on the elongation is studied for tube sinking. A representation of the elongation evolution is given in Fig. 11. This graph is actually obtained with the same simulations as in Section 4.2.

The elongation increases with the relative thickness in a quite linear way. In fact, the greater the relative thickness, the greater the area reduction. Thus, due to volume conservation, the tube is more stretched. This figure also reveals that the outer and inner surfaces have the same elongation, even if the outer one is constrained by the die and the inner is free to deform.

Please cite this article in press as: F. Boutenel et al., Finite element modelling of cold drawing for high-precision tubes, C. R. Mecanique (2018), https://doi.org/10.1016/j.crme.2018.06.005

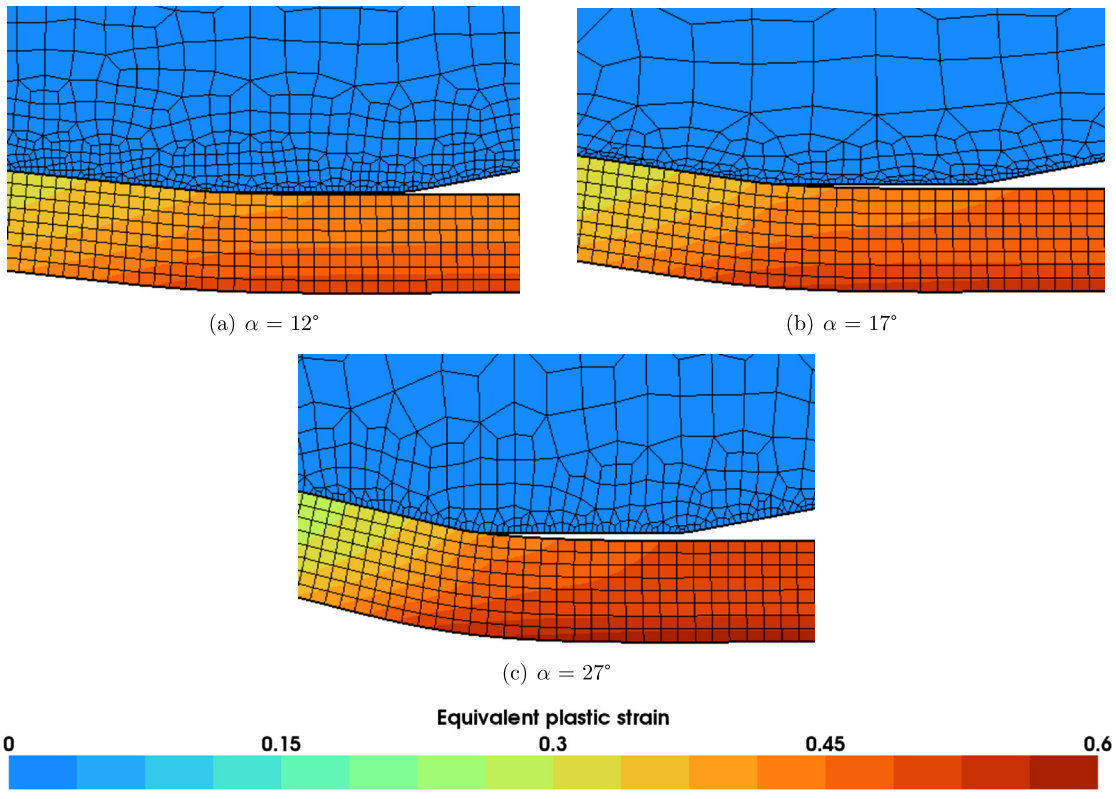

Fig. 9. Equivalent plastic strain of the tube for three values of the die angle, at the steady state (tube sinking case).

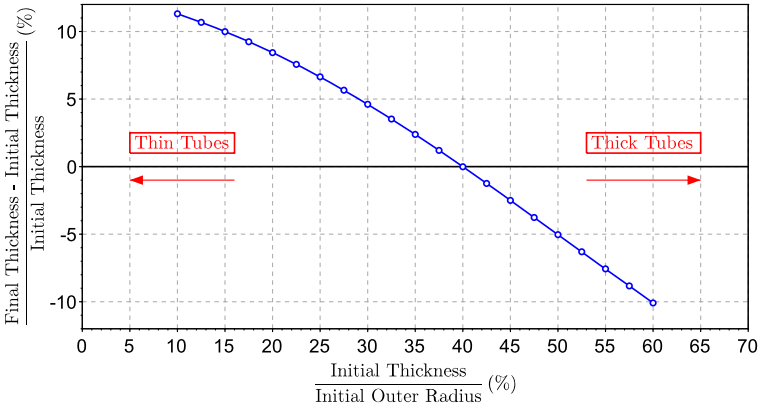

Fig. 10. Influence of the relative thickness on the final tube thickness (tube sinking case).

4.4. Distribution of residual stresses in the tube thickness

The tube is subjected to strain hardening during cold tube drawing. An analysis of the residual stresses through the thickness allows us to understand the tube state at the end of the drawing. Fig. 12 gives an example for tube sinking (Test 1).

The evolution of the von Mises stress through the thickness reveals that the tube is more constrained on its inner surface than on its outer one. Then, shear and radial stresses are not significant. Moreover, the circumferential stress is negative in the inner part of the tube, and positive in the outer one. Finally, as far as the longitudinal stress is concerned, the tube is in compression on its inner surface and in traction on its outer one.

Please cite this article in press as: F. Boutenel et al., Finite element modelling of cold drawing for high-precision tubes, C. R. Mecanique (2018), https://doi.org/10.1016/j.crme.2018.06.005

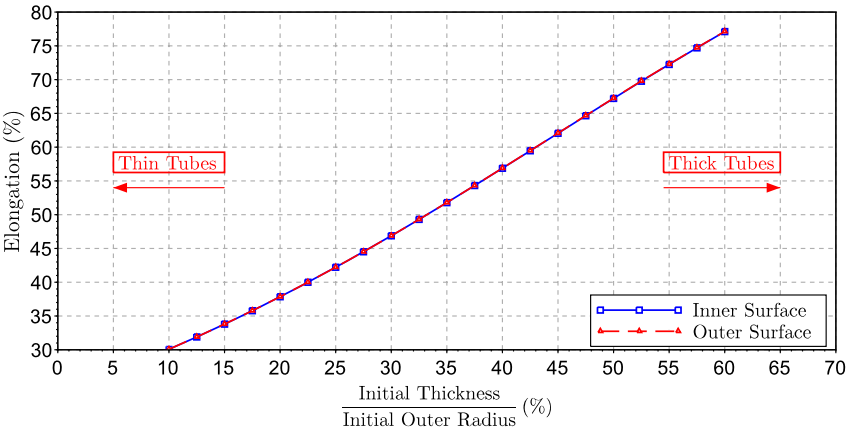

Fig. 11. Elongation as a function of the initial relative thickness of the tube (tube sinking case).

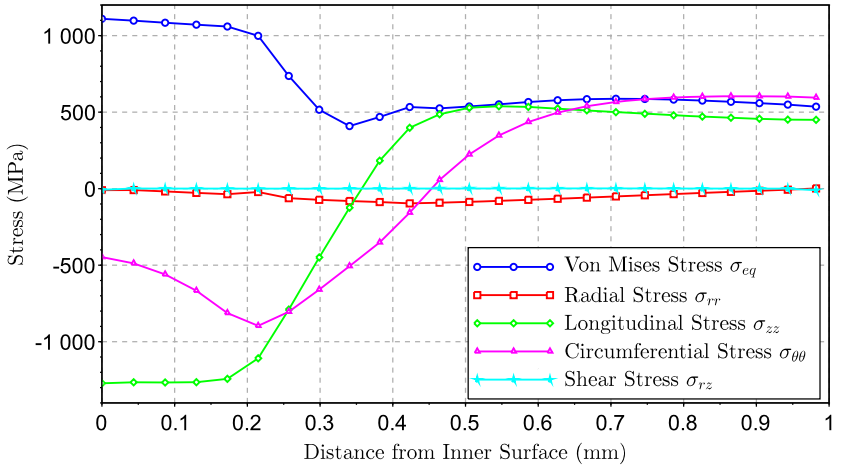

Fig. 12. Distribution of the residual stresses in the thickness for tube sinking.

Table 11
Mandrel drawings of Tubes A and B before the reeling operation – extracted from [4].

Tube	Die			Mandrel	Speed
	D_{die} (mm)	L_b (mm)	α (deg)	D_m (mm)	(m·min^{-1})
A	7.48	0.9	22.7	6.50	11.4
B	8.13	0.3	33.0	7.00	11.4

Tube	Initial tubes (mm)			Final tubes (mm)		
	Outer ∅	Thickness	Inner ∅	Outer ∅	Thickness	Inner ∅
A	9.05	0.64	7.77	7.52	0.51	6.50
B	10.50	0.75	9.00	8.16	0.58	7.00

4.5. Prediction of the reeling operation

In the case of mandrel drawing, the tube is clamped around the mandrel at the end of the process. A reeling operation is needed to remove the mandrel from the tube. It consists in relaxing the tube stresses thanks to a roller system.

In practical, this operation is difficult to perform on some tubes. Even if the reeling operation is not simulated with this model, a qualitative study is proposed in this section, to predict the difficulty of the reeling operation of two tubes.

The experiments have showed that the reeling operation of Tube B is more difficult than the one of Tube A. The characteristics of the drawings preceding the reeling operation are presented in Table 11.

Please cite this article in press as: F. Boutenel et al., Finite element modelling of cold drawing for high-precision tubes, C. R. Mecanique (2018), https://doi.org/10.1016/j.crme.2018.06.005

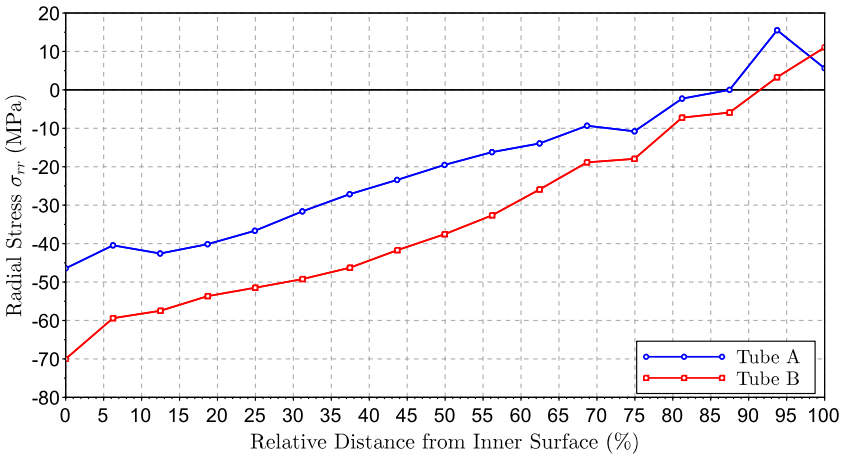

Fig. 13. Repartition of the radial stress before the reeling operation.

Considering that the clamping on the mandrel is due to the residual radial stress, the idea is to compare the distribution of this stress through the final section after drawing for both tubes. Fig. 13 represents the repartition of radial stress in the thickness for Tubes A and B.

For both tubes, the radial stress is negative, except on the outer skin. This compression is coherent with the tube clamping observed in practice. It can also be observed that the compression is more important in Tube B than in Tube A (by a factor of 1.55 on the inner skin). As a consequence, a greater relaxation is necessary for Tube B. Thus simulation confirms that removing the mandrel from Tube A by a reeling operation is easier than doing the same from Tube B.

Of course, the results of this qualitative study should be ideally confirmed by a full simulation of the removal process. The simulation of this complete post-operation will be investigated in future models.

5. Conclusions

A finite element model of cold tube drawing has been presented in this paper. Also, the numerical parameters have been chosen to assure the reliability of the model.

Then, drawing experiments have been achieved and compared to simulations in order to validate the model. This showed that the final dimensions of the tube can be predicted by the model with a good accuracy.

Furthermore, a complete analysis of the process has been presented. It has been shown that the die angle has an influence on the drawing force. Also, the relative thickness has an impact on the mechanical behaviour of the tube during the drawing operation. In fact, it can become thicker or thinner, depending on whether relative thickness is below or above a transition value (which is 40% in the presented case). Moreover, the tube elongation, identical on inner and outer surfaces, increases with relative thickness. Finally, an analysis of the residual stresses allowed us to understand the tube state at the end of drawing. In particular, it can qualify the difficulty of the reeling operation in the case of mandrel drawing.

As part of the optimisation of the process parameters, this first work gives us promising results. Other studies will be considered in future works: thermal effects, anisotropy of the tube material and chaining several successive drawing operations.

Acknowledgements

We sincerely wish to thank the French company Minitubes, which supported and contributed to this work.

References

[1] P. Poncin, D. Ferrier, A. Loshakove, J. Proft, C. Meyer-Kobbe, A comparison between two manufacturing methods, in: A.P.S. Russell (Ed.), Proceedings of the International Conference on Shape Memory and Superelastic Technologies, Asilomar, California, May 2000, 2000, p. 477.

[2] U. Amborn, S. Ghosh, I. Leadbetter, Modern side-shafts for passenger cars: manufacturing processes II – Monobloc tube shafts, J. Mater. Process. Technol. 63 (1) (1997) 225–232, https://doi.org/10.1016/S0924-0136(96)02746-X.

[3] K. Yoshida, H. Furuya, Mandrel drawing and plug drawing of shape-memory-alloy fine tubes used in catheters and stents, J. Mater. Process. Technol. 153 (2004) 145–150, https://doi.org/10.1016/j.jmatprotec.2004.04.182.

[4] M. Palengat, Modélisation des couplages multiphysiques matériaux–produits–procédés lors de l'étirage de tubes : application aux alliages métalliques usuels, Ph.D. thesis, Université de Grenoble, France, 2009 (in French).

[5] K.-K. Um, D.N. Lee, An upper bound solution of tube drawing, J. Mater. Process. Technol. 63 (1) (1997) 43–48, https://doi.org/10.1016/S0924-0136(96)02597-6.

[6] N. Alexandrova, Analytical treatment of tube drawing with a mandrel, Proc. Inst. Mech. Eng., C J. Mech. Eng. Sci. 215 (5) (2001) 581–589, https://doi.org/10.1243/0954406011520968.

[7] N. Alexandrova, Fracture analysis of tube drawing with a mandrel, J. Mater. Process. Technol. 142 (3) (2003) 755–761, https://doi.org/10.1016/S0924-0136(03)00618-6.
[8] D. Zhao, H. Du, G. Wang, X. Liu, G. Wang, An analytical solution for tube sinking by strain rate vector inner-product integration, J. Mater. Process. Technol. 209 (1) (2009) 408–415, https://doi.org/10.1016/j.jmatprotec.2008.02.011.
[9] K. Sawamiphakdi, G. Lahoti, P. Kropp, Simulation of a tube drawing process by the finite element method, J. Mater. Process. Technol. 27 (1) (1991) 179–190, https://doi.org/10.1016/0924-0136(91)90052-G.
[10] C. Linardon, D. Favier, G. Chagnon, B. Gruez, A conical mandrel tube drawing test designed to assess failure criteria, J. Mater. Process. Technol. 214 (2) (2014) 347–357, https://doi.org/10.1016/j.jmatprotec.2013.09.021.
[11] P. Karnezis, D. Farrugia, Study of cold tube drawing by finite-element modelling, J. Mater. Process. Technol. 80 (1998) 690–694, https://doi.org/10.1016/S0924-0136(98)00127-7.
[12] M. Palengat, G. Chagnon, D. Favier, H. Louche, C. Linardon, C. Plaideau, Cold drawing of 316L stainless steel thin-walled tubes: experiments and finite element analysis, Int. J. Mech. Sci. 70 (2013) 69–78, https://doi.org/10.1016/j.ijmecsci.2013.02.003.
[13] J.-J. Sheu, S.-Y. Lin, C.-H. Yu, Optimum die design for single pass steel tube drawing with large strain deformation, Proc. Eng. 81 (2014) 688–693, https://doi.org/10.1016/j.proeng.2014.10.061.
[14] S.-K. Lee, M.-S. Jeong, B.-M. Kim, S.-K. Lee, S.-B. Lee, Die shape design of tube drawing process using Fe analysis and optimization method, Int. J. Adv. Manuf. Technol. 66 (1) (2013) 381–392, https://doi.org/10.1007/s00170-012-4332-8.
[15] J.-F. Béland, M. Fafard, A. Rahem, G. D'Amours, T. Côté, Optimization on the cold drawing process of 6063 aluminium tubes, Appl. Math. Model. 35 (11) (2011) 5302–5313, https://doi.org/10.1016/j.apm.2011.04.025.
[16] S. Kim, Y. Kwon, Y. Lee, J. Lee, Design of mandrel in tube drawing process for automotive steering input shaft, J. Mater. Process. Technol. 187 (2007) 182–186, https://doi.org/10.1016/j.jmatprotec.2006.11.134.
[17] METAFOR website, University of Liège, Belgium, http://metafor.ltas.ulg.ac.be/.
[18] L. Noels, L. Stainier, J.-P. Ponthot, Simulation of crashworthiness problems with improved contact algorithms for implicit time integration, Int. J. Impact Eng. 32 (5) (2006) 799–825, https://doi.org/10.1016/j.ijimpeng.2005.04.010.
[19] L. Adam, J.-P. Ponthot, Numerical simulation of viscoplastic and frictional heating during finite deformation of metal. Part I: theory, J. Eng. Mech. 128 (11) (2002) 1215–1221, https://doi.org/10.1061/(ASCE)0733-9399(2002)128:11(1215).
[20] ASTM F138-00: Standard Specification for Wrought 18 Chromium–14 Nickel–2.5 Molybdenum Stainless Steel Bar and Wire for Surgical Implants (UNS S31673), https://doi.org/10.1520/F0138-00.
[21] S. Fréchard, A. Redjaïma, G. Metauer, E. Lach, A. Lichtenberger, Comportement dynamique et évolution microstructurale d'un acier inoxydable austénitique allié à l'azote, in: Matériaux 2002, Tours, France, 2002 (in French).
[22] G. Johnson, W. Cook, A constitutive model and data for metals subjected to large strains, high strain rates, and high temperatures, in: Proceedings of the 7th International Symposium on Ballistics, The Hague, Netherlands, 19–21 April 1983, 1983, pp. 541–547.
[23] P. Joyot, Modélisation numérique et expérimentale de l'enlèvement de matière : application à la coupe orthogonale, Ph.D. thesis, Université Bordeaux-1, Bordeaux, France, 1994 (in French).
[24] C. Linardon, Precision Tube Drawing for Biomedical Applications: Theoritical, Numerical and Experimental Study, Ph.D. thesis, Université de Grenoble, France, 2013.
[25] N. Sandru, G. Camenschi, A mathematical model of the theory of tube drawing with floating plug, Int. J. Eng. Sci. 26 (6) (1988) 569–585, https://doi.org/10.1016/0020-7225(88)90055-9.
[26] J. Chung, G. Hulbert, A time integration algorithm for structural dynamics with improved numerical dissipation: the generalized-α method, J. Appl. Mech. 60 (2) (1993) 371–375, https://doi.org/10.1115/1.2900803.

Please cite this article in press as: F. Boutenel et al., Finite element modelling of cold drawing for high-precision tubes, C. R. Mecanique (2018), https://doi.org/10.1016/j.crme.2018.06.005